DNA groove binding of an asymmetric cationic porphyrin and its Cu(II) complex: Resolved by spectroscopic, viscometric and molecular docking studies

Roghayeh Aleeshah, Abbas Eslami[*]

Department of Inorganic Chemistry, Faculty of Chemistry, University of Mazandaran, Babolsar, Iran

Abstract

In the present study, the interaction between water-soluble cationic asymmetric porphyrin, 5-(1-Hexadecyl pyridinium-4-yl)-10, 15, 20-tris (1-Butyl pyridinium-4-yl) Porphyrin Chloride, and its copper (II) derivative with calf thymus DNA (CT-DNA) were studied by means of spectroscopic techniques, viscosity measurements and molecular docking. The monitoring of the changes in visible absorbance spectra showed a small red shift and a little hypochromicity in the Soret band. Also, no significant changes were appeared in the viscosity of DNA with increasing of the porphyrins. These results suggested that these porphyrins bound to DNA through the groove binding mode. Then, multivariate curve resolution-alternating least squares (MCR-ALS) method was employed on UV–visible spectral data matrix to resolve the spectral and concentration profiles of the components involved in the interaction and the binding constant was estimated by the combination of bard equation and MCR-ALS approach. Furthermore, molecular docking studies confirmed experimental results obtained by spectral techniques and provide deeper insight into the porphyrin-DNA interaction.

Keywords: Calf thymus DNA, Asymmetric cationic porphyrin, Grove binding mode, MCR-ALS, Molecular docking.

1. Introduction

The natural porphyrins, metalloporphyrins, and related compounds are of central importance to many vital biological processes. Porphyrin-based systems have been widely studied due to their photophysical and electrochemical properties as well as optoelectronic applications [1, 2]. The unique and inherent chemical characteristics of porphyrins make them appropriate candidates for photodynamic therapy (PDT) [3], ion sensors [4], magnetic resonance imaging (MRI) [5], electrocatalysis [6], photocatalysis [7], non-linear optics [8], chemical sensors [9], photovoltaic cells [10] and so on [11].

Interaction of small molecules with deoxyribonucleic acid (DNA), as a target molecule for specific drugs, has attracted considerable interest in recent years due to their substantial roles in biological systems.

[*].Corresponding author: Department of Inorganic Chemistry, Faculty of Chemistry, University of Mazandaran, Babolsar, Iran.
E-mail address: eslami@umz.ac.ir; eslami_a@yahoo.co.uk

Porphyrins bind to DNA, then the target site of DNA molecules modifies photodynamically or chemically by cleaving nucleic acid and can be used as a chemical probe of DNA [12, 13].

The interaction of porphyrins with DNA has been widely investigated by means of UV-visible absorption spectroscopy [14], circular dichroism [15], fluorescence [16], viscosity [17], Nuclear magnetic resonance (NMR) spectroscopy [18] and X-ray crystallography [19]. Water-soluble cationic porphyrins can bind with DNA through noncovalent interactions in three ways: outside binding accompanied by the self-stacking along the polynucleotide helix, groove binding interaction, and intercalation binding. The porphyrin-DNA binding modes depend on both the electronic structure of the porphyrin and the position and size of the substituents [20]. Metalloporphyrin derivatives of meso-tetra (N-methyl-4-pyridinium) porphyrin (H_2TMPyP) with square planar geometry such as Cu(II) and Ni(II) complexes can intercalate between two adjacent base pairs of DNA, whereas related Zn(II) and Co(II) derivatives are capable of outside binding to the DNA duplex owing to axial aqua ligands [21]. Additionally, the 3D structure of DNA molecule entirely depends on the physicochemical properties of the surrounding environment. So the binding mode is affected by other conditions such as salt concentration, pH, temperature and the base pairs sequences [22].

In this study, MCR-ALS method was applied to the study of DNA-ligand interactions [23]. The binding constant of DNA-ligand interaction was estimated by the combination of bard equation and MCR-ALS. The observed limitations in biological systems are constituted by more than two components, such as overlapping of signals, can be resolved using MCR-ALS [24]. The concentration profiles are attained by performing MCR-ALS on the experimental data matrix. The concentration profiles provide suitable information about the interaction mechanism and chemically active species involved [25].

For the preparation of asymmetric porphyrins (porphyrins bearing various substituents at the meso-positions), different synthetic routes were reported

[26]. The most common synthetic route for the preparation of asymmetrical cationic porphyrins with three identical substituents (AB_3- porphyrins) is the partial modification of a porphyrin bearing four identical meso substituents in high yield. In the present work, we synthesized asymmetric metalloporphyrin derivative of Cu(II) containing 5-(1-Hexadecyl pyridinium-4-yl)-10, 15, 20- tris (1-Butyl Pyridinium-4-yl) Porphyrin Chloride (MHxTB) ligand in good yield according to our pervious study [27]. The effect of bulky group substitution on the DNA binding with porphyrin was studied by absorption spectroscopy, resonance light scattering spectroscopy, circular dichroism, emission spectroscopy and also dynamic viscosity measurements. The results illustrated that these porphyrins have a high binding affinity toward CT-DNA and bind to it through outside mode. Furthermore, molecular docking was applied to understand the most probable mode of DNA binding.

2. Experimental

2.1. Materials and Apparatus

All of the chemicals were used as received from commercial sources without further purification.

^{1}H-NMR spectra were recorded using a Bruker Avance DRX-400 spectrometer. Elemental analysis for C, H, and N was carried out with a LECO 600 elemental analyzer. Electronic spectral measurements were performed using a UV-Vis Braic 2100 double beam spectrophotometer. Emission spectra were recorded with a Perkin-Elmer LS-5B fluorescence spectrophotometer in tris buffer solution by 1 cm path length quartz cell. CD measurements were carried out using a Model 215 CD spectrometer. The viscometric measurement was performed with a Lovis 2000 M/ME microviscometer.

2.2. Synthesis and characterization

2.2.1. Synthesis of 5-(1-Hexadecyl pyridinium-4-yl)-10, 15, 20-tri (Pyridyl) Porphyrin Bromide (MHxPyPBr), 1

Meso-tetra(4-pyridyl)porphyrin was prepared and purified previously published protocol [28]. Then hexadecane (2.3 mL, 7 mmol) and TPyP (0.4 g, 0.65 mmol) were dissolved in 400 ml of absolute

ethanol/chloroform (1:3, v/v). The solution was refluxed at 75°C under N_2 atmosphere in the dark for 6 days. The reaction mixture was cooled, and was evaporated under reduced pressure. The crude residue was placed in column chromatography on silica gel, eluted with chloroform/ethanol (8:2, v/v) and then, it was recrystallized from chloroform to acquire porphyrin **1** (yield 30%), mp >300 °C. ^{1}H NMR (CDCl$_3$, 400 MHz) δ ppm: -2.94(s, 2H, NH), 0.85(t, 3H, CH$_{3(hexadecyl)}$), 1.6-1.1(m, 26H, CH$_{2(hexadecyl)}$), 2.36 (m, 2H, β-CH$_{2(hexadecyl)}$), 5.32 (t, 2H, α-CH$_{2(hexadecyl)}$), 7.9 (d, 4H, H$_{m\text{-}py.}$), 8.13 (d, 2H, H$_{m\text{- N-hexadecylpy.}}$), 8.89-9.07 (m, 16H, H$_{pyrr.}$, H $_{o\text{-N-hexadecylpy.}}$ and H$_{opy}$), 9.79 (d, 2H, H$_{o\text{-N-hexadecylpy}}$).

2.2.3. Synthesis of 5-(1-Hexadecyl pyridinium-4-yl)-10, 15, 20-tris (1-Butyl Pyridinium-4-yl) Porphyrin Chloride (MHxTB), 2

The mixture of MHxPyPBr (0.3 g, 0.32 mmol) and 1-bromobutane (3 mL, 27.93 mmol) in dimethylformamide (15 mL) and acetonitrile (35 mL) was refluxed in the dark at 110°C for 72 h under N_2 atmosphere. After cooling the reaction mixture to room temperature, the excess 1-bromobutane was removed by adding diethyl ether. The obtained precipitate was washed with diethyl ether, dried in a vacuum desiccator, dissolved in methanol. and passed over an anionic exchange resin for 2 days to get chloride salt of $C_{55}H_{60}N_8Cl_4, 8H_2O$. The obtained purple powder was dried over P_2O_5 in vacuum for one week (yield 97%), mp > 300°C. FT-IR (KBr, ν, cm^{-1}): 3435 (N-H$_{str.}$), 2922 (C-H $_{str.Ar.}$), 2853 (C-H $_{str.ali.}$), 1555 (C=C $_{str.}$), 1469 (C=N), 961(N-H$_{bend.}$), 792, 723 (C–H $_{bend.}$). ^{1}H NMR (DMSO, 400 MHz) δ ppm: 9.58 (d, 6H, H$_{o\text{-N-hexadecylpy}}$), 9.49 (d, 2H, H$_{o\text{-N-methylpy}}$), 9.23 (s, 6H, , H$_{pyrr.}$), 9.03 (m, 8H, H$_{pyrr.}$), 8.19 (s, 2H, H$_{m\text{-py.}}$), 4.98 (t, 6H, α-CH$_{2(butyl)}$), 4.73 (t, 2H, α-CH$_{2(hexadecyl)}$), 2.56 (m, 6H, β-CH$_{2(butyl)}$), 2.50 (m, 2H, β-CH$_{2(hexadecyl)}$), 2.3 (m, 8H, γ-CH$_{2(hexadecyl)}$, β-CH$_{2(butyl)}$), 1.65-1.1 (m, 24H, CH$_{2(hexadecyl)}$), 0.84 (m, 12H, CH$_{3(hexadecyl}$, CH$_{3(butyl)}$), -2.97 (s, 2H, NH). Anal. Calc. For $C_{68}H_{86}N_8Cl_4$ (MW (MHxTB)) = 1154.57 g.mol^{-1}): C, 70.57; H, 7.49; N, 9.68%. Found: C, 70.8; H, 7.6; N, 9.7%. UV-Vis (H$_2$O) λ nm (ε (M^{-1}cm^{-1}): 426 (107.6× 10^3), 518 (7.32×

10^3), 555 (3.32× 10^3), 584 (3.12× 10^3), 644 (0.89 × 10^3).

2.2.4. Synthesis of Cu (II) 5-(1-Hexadecyl pyridinium-4-yl)-10, 15, 20-tris (1-Butyl Pyridinium-4-yl) Porphyrin Chloride, 3

To a solution of porphyrin **2** (0.05 g, 0.043 mmol) in 25 mL of distilled water was added Cu(CH$_3$COO)$_2$ (0.37 g, 2.1 mmol) under N_2 atmosphere. The reaction mixture was allowed to reflux for 24 h. After cooling, a solution of saturated KClO$_4$ was added to the mixture, then resulting precipitate was washed with cold diethyl ether and dilute aqueous KClO$_4$ solution, dissolved in methanol and passed over an anionic exchange resin for 2 days to get CuMHxTB chiorid salt. The obtained aqueous solution was dried in vacuum at 40°C to get porphyrin **3** (yield 92%), mp >300 °C. FT-IR (KBr, ν, cm^{-1}): 2923 (C-H$_{str.Ar.}$), 2850 (C-H $_{str. ali.}$), 1555 (C=C $_{str.}$), 1460 (C=N), 1005 (Cu-N), 790, 721 (C–H $_{bend.}$).UV-Vis (H$_2$O) λ nm (ε (M^{-1}cm^{-1}): 428 (217× 10^3), 546 (19.2× 10^3), 590.6 (2.94× 103).

2.4. DNA binding studies

DNA stock solutions were prepared by dissolving CT-DNA in Tris-HCl buffer at pH 7.10 and stored at 4 °C for 24 hours. The absorbance ratio (A$_{260}$/A$_{280}$) equals to 1.8 that specified the purity of DNA from protein [29]. Then the extinction coefficient of ε=6600 M^{-1} cm^{-1} at 260 nm was applied to define spectrophotometrically the concentration of DNA solutions that used in various experiments [30].

2.4.1. Spectroscopic measurements

CT-DNA solution was added into a constant concentration of the mentioned porphyrins (9.01×10^{-6} M and 4.6×10^{-6} M for porphyrin **2** and **3**, respectively). Five minutes after each injection, UV-Vis spectra were registered at 20°C.

Emission spectra of porphyrin **2** were recorded at 20°C in the range of 600 to 750 nm.

Induced CD spectra were recorded for porphyrins **2** and **3** at the mole ratios of 0.9 porphyrin to DNA over the spectral range of 380-600 nm at 20°C.

RLS spectra were scanned in the region from 300 to 700 nm at 20°. Then, the obtained data were corrected to get the "pure" scattering component.

2.4.2. Multivariate curve resolution

The soft modeling-based MCR–ALS procedure was performed to decompose spectroscopic data into the concentration profiles and pure spectra [31]. The experimental data matrix D (i × j) was decomposed into C (i × n) and S^T (n × j) based on the bilinear model according to the following equation:

$$D_{(i \times j)} = C_{(i \times n)} S^T_{(n \times j)} + E_{(i \times j)} \qquad (1)$$

where S, C and E are pure spectra, pure concentration profiles and residuals matrix, respectively.

MCR-ALS procedure is consist of following step:

1. Data matrix arrangement
2. Determination of the number of component by applying singular value decomposition (SVD)
3. The initial estimation of C or S^T (equations 2 and 3) [32]
4. Applying constraint and optimization parameters [33]

$$S^T = (C)^+ D \qquad (2)$$

$$C = D(S^T)^+ \qquad (3)$$

where $(C)^+$ and $(S^T)^+$ are C matrices and the pseudoinverse of the S^T, respectively [34, 35]. The percentage of lack of fit (LOF) (Eq. 4) and the explained data variance (R^2) parameters (Eq. 5) are calculated to evaluate, which the experimental data were well fitted [36].

$$lof(\%) = 100 \sqrt{\frac{\sum_{ij} e^2_{ij}}{\sum_{ij} d^2_{ij}}} \qquad (4)$$

$$R^2 = 100 \sqrt{\frac{\sum_{ij} d^2_{ij} - \sum_{ij} e^2_{ij}}{\sum_{ij} d^2_{ij}}} \qquad (5)$$

where d_{ij} is an element of the input data matrix D and e_{ij} is the related residual acquired from the discrepancy between the input element and the MCR reproduction.

2.4.3. Viscosity Measurements

The DNA solutions containing various concentrations of porphyrins were prepared for investigating the effect of the presence porphyrin on the relative viscosity of DNA at 20.0 ± 0.1 °C.

2.4.4. Molecular docking

Molecular docking studies were performed using AutoDock 4.2 program to get more evidence for the accuracy of the above results [37]. To perform molecular docking, the structure of porphyrins **2** and **3** were optimized using DMOL3 program that employed in Materials Studio package. The geometric optimization is performed with DNP basis sets based on the generalized gradient approximation (GGA) [38]. The optimized geometry was docked into DNA fragments that its crystal structure was downloaded from Protein Data Bank (PDB ID: 1BNA) (*http://www. rcsb.org*). Then, the MGL Tools 1.5.4 package was used to convert PDB files to pdbqt format. The grid maps were fixed by centering the grid box on either the groove or the intercalation site and comprised of $60 \times 70 \times 60$ points of 0.375 Å spacing. All other parameters were left at the default values. Lamarckian genetic algorithm (LGA) method was employed to study molecular docking simulation [39].

3. Results and Discussion

3.1. Synthesis

In this present study, we reported the synthesis of asymmetric cationic 5-(1-Hexadecyl pyridinium-4-yl)-10, 15, 20-tris (1-Butyl Pyridinium-4-yl) Porphyrin Chloride, **2** (Fig. 1).
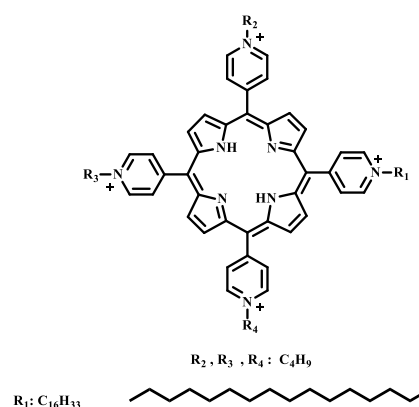
Fig. 1. Chemical structures of porphyrin **2**

The route for the synthesis of porphyrin **2** is shown in Scheme 1s. In the first step, after the purification of meso-tetra(pyridyl) porphyrin according to the previous reports [28], a mixture of 1-bromohexadecane and TPyP was refluxed in chloroform and ethanol for 6 days at 75°C for attaching one hexadecyl group to the N-position of the peripheral pyridyl groups. The reaction mixture showed three bands on the TLC plate, the second separated component was collected, purified and recrystallized from chloroform to afford porphyrin **1**

(45% yield). In the next step, the porphyrin **2** was synthesized through tri N-alkylation of the porphyrin **1** by a large excess of 1-bromobutane at 110 °C for 2 days. The reaction product was passed over an anionic exchange resin to afford the desired chloride salt of the porphyrin **2**. ^{1}H NMR, UV–visible spectroscopy and elemental analysis verified their structure (Fig. 1s-4s). In the IR spectrum of porphyrin **2**, the absorption bands at 3435 and 961 cm^{-1} are attributed to N–H stretching (in planarity) and bending (out of planarity) vibrations of free base porphyrin. These absorption bands disappeared in the spectra of porphyrin **3**, after the metal insertion reactions, a new strong absorption band appeared at 1005 cm^{-1}, which further confirmed the formation of metal complex. In the ^{1}H-NMR spectrum of porphyrin **2**, the signals of the two inner N-H groups (the shielded N-H protons) appear at very high field (-2.97 ppm) because of the anisotropic effect from the porphyrin ring current. The triplet signal was appeared at 4.73 ppm due to α-CH$_{2(\text{hexadecyl})}$ which clarified the formation of porphyrin **1.** The presence of a triplet peak at 4.98 ppm was assigned to α-CH$_{2(\text{t-butyl})}$ that approved the formation of the porphyrin **2.** The absorption spectrum of porphyrin **2** consists of a strong Soret band at 426 nm, and four less intense Q bands in the visible region (518, 555, 584 and 644 nm). Metalloporphyrin **3** demonstrated a strong Soret band at 428 nm and two weak Q-bands in visible region (546 and 590 nm). The difference between the absorption spectra of the porphyrin **2** and metalloporphyrin **3** is assigned to the C$_1$ symmetry of the free-base porphyrin which is due to inner proton and C$_s$ symmetry of metalloporphyrin. The intense soret band is attributed to the S$_0$ to S$_2$ transition whereas the Q bands are attributed to the S$_0$ to S$_1$ transition. The soret and the Q bands both arise from π–π* transitions and can be explained by the Gouterman four orbital model. Cu (II) metalloporphyrin **3** absorption peaks are shifted to the shorter wavelength than free base porphyrin **2** due to metal dπ (d$_{xz}$ and d$_{yz}$) to prophyrin π* back bonding. This results in an increased porphyrin π to π* energy separation causing the electronic absorptions to undergo hypsochromic (blue) shifts.

3.2. Spectroscopic studies

A wide investigation has been carried out on the interaction of porphyrin with DNA [40] and the results illustrated that the binding constant depends on the DNA sequence, DNA structure, porphyrin structure, and experimental conditions. To get further information about porphyrin-DNA interaction, spectrophotometric titration of porphyrins is commonly carried out by DNA in a buffer solution. The intensity and magnitude of the Soret band is effective for estimating the binding constants and distinguishing the binding mode (intercalative and outside binding) [41].

UV–Vis absorption spectroscopy is a conventional analytical technique in the investigation of porphyrin-DNA interaction [42]. UV-Visible spectra of porphyrins **2** and **3** during titration with CT-DNA were depicted in Fig. 2a and 2b, respectively. At low ($\frac{[\text{DNA}]}{[\text{porphyrin}]}$) mole ratio, little changes were appeared in the Soret band that can be related to weak aggregations of porphyrin on the surface of DNA. Then, the intensity of Soret peak was major decreased, hypochromic effect and a bathochromic shift were appeared for porphyrins that due to the porphyrin-DNA interaction with further addition of DNA.

Then, MCR-ALS method was applied on the optical absorption data to estimate binding constant. The presence of two components and the initial spectra were estimated by employing SVD and OPA algorithm, respectively. Then the non-negativity, unimodality, closure constraint and selection of optimization parameters were employed in the ALS optimization to acquire the concentration and spectra profiles (in Fig. 3 and 4). The standard deviation of the residuals was 0.013 and 0.008 for porphyrins 2 and 3, respectively. The LOF was obtained 5.664 and 2.771 for porphyrins 2 and 3, respectively.

absorption spectra for porphyrins **2** and **3**, respectively.
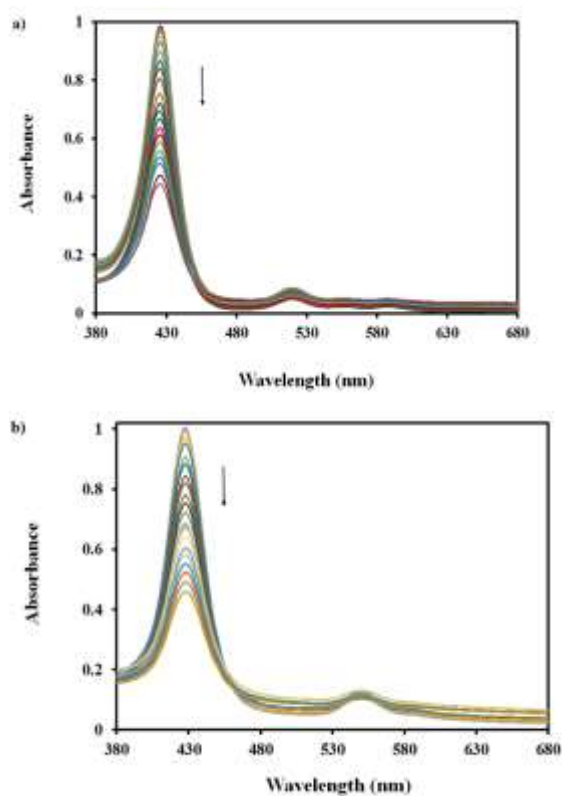
Fig. 2. Changes in absorption spectra of porphyrin upon progressive addition of DNA solution at 20 ºC in 10 mM Tris-HCl/25 mM NaCl (pH=7.1) buffer. a) [porphyrin **2**]= 9.01× 10⁻⁶ M, [DNA]= (0-1.87) × 10⁻⁵ M, b) [porphyrin **3**]= 4.60× 10⁻⁶ M), [DNA] = (0-1.78) × 10⁻⁵ M

The binding constant was estimated by the combination of bard equation and MCR-ALS [24, 43]. The bard equation can be exhibited by the following equation:
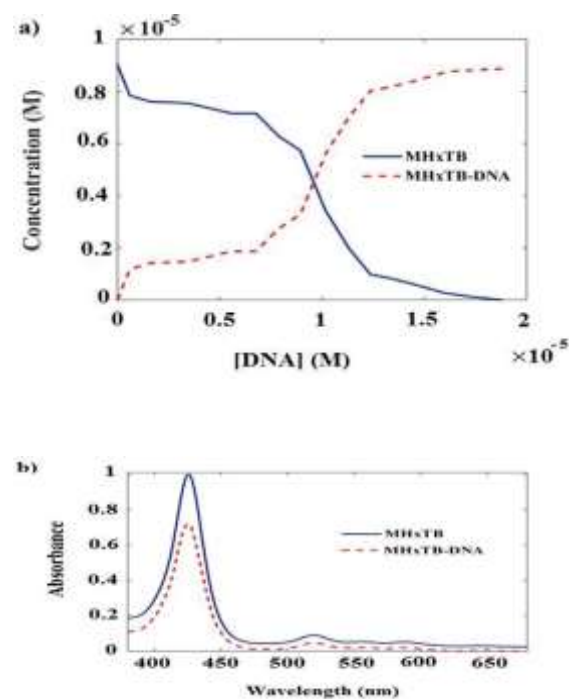
$$\frac{(\varepsilon_a - \varepsilon_f)}{(\varepsilon_b - \varepsilon_f)} \qquad (6)$$

$$= \frac{[b - (b^2 - 2k_b + \frac{c_t[DNA]}{n})^{1/2}]}{(2k_a c_t)}$$

$$b = 1 + 2k_b c_t + k_b \frac{[DNA]}{2} \qquad (7)$$

where ε_a, ε_f, ε_b are the apparent extinction coefficient, the extinction coefficient for the free porphyrin, and the bound form, C_t is the concentration of free porphyrin; [DNA] is the DNA concentration expressed in nucleotide phosphate, n is the binding site size, and K_b is the binding constant. The estimated binding constants are given in Table 1. These porphyrins represented slightly red shift about 2 and 4 nm with a hypochromicity of 9.85% and 6.91% in

Fig. 3. Results obtained from analysis of the visible absorption data recorded during interaction MHxTB with DNA solution at 20°C in Tris-HCl buffer by MCR-ALS. Extracted concentration (a) and pure spectra (b) profiles for MHxTB and MHxTB-DNA complex
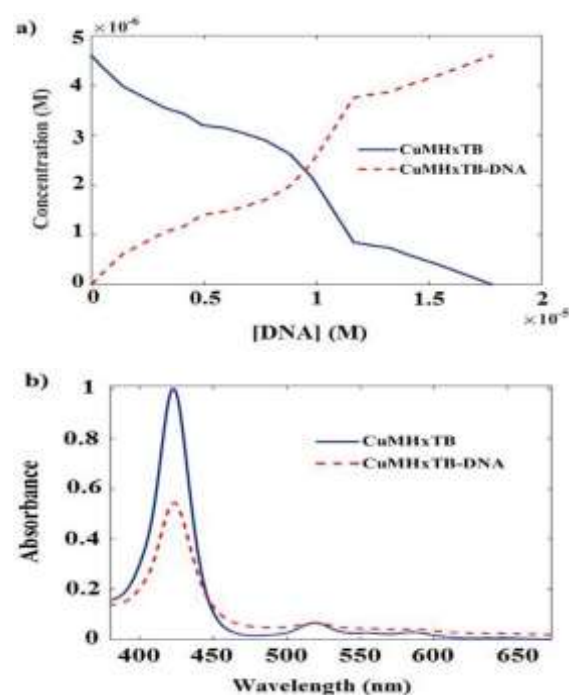
Fig. 4. Results obtained from analysis of the visible absorption data recorded during interaction CuMHxTB with DNA solution at 20°C in Tris-HCl buffer by MCR-ALS. Extracted concentration (a) and pure spectra (b) profiles for CuMHxTB and CuMHxTB-DNA complex

Table 1. Binding parameters of the interaction between porphyrin and CT-DNA at 20°C.

| Compound	λ_{max} (nm)/[$\varepsilon \times 10^{-4}$ (M^{-1} cm^{-1})]		H% [a]	n	$K_b \times 10^{-4}$ (M^{-1})
	free	DNA binded			
Porphyrin 2	426 [10.76]	428 [9.7]	9.85	0.3	8.7
Porphyrin 3	428 [21.7]	432[20.2]	6.91	0.2	7.6

[a] H%: Hypochromicity is defined as $H\% = \frac{(\varepsilon_f - \varepsilon_b)}{\varepsilon_f} \times 100$ where ε_f and ε_b are the molar absorption coefficients for the free and bound forms.

The emission spectrum of interaction porphyrin 3 with CT-DNA is demonstrated in Fig. 5. Porphyrin **2** emitted light because of a highly conjugated double-bond structure, but Porphyrin **3** didn't emit light due to paramagnetic metal ion. In the absence of CT-DNA, porphyrin **2** solution displays a strong Q (0,0) band, and a weak shoulder corresponds to Q (1,0) in 652 and 710 nm, respectively. Upon addition of CT-DNA to porphyrin **2** solution**,** the fluorescence intensity was smoothly decreased, but the fluorescence intensity was dramatically increased by further addition of DNA to the solution. The initial decrease in the fluorescence intensity may be related to aggregate porphyrin **2** on the CT-DNA surface. In higher concentrations, the enhancement of the fluorescence intensity is due to binding of porphyrin **2** monomer to CT-DNA. The linear Stern–Volmer quenching constant was calculated according to the following equation [44]:

$$\frac{F_0}{F} = 1 + K_{SV}[Q] \qquad (8)$$

where F_0 and F are the fluorescence intensities in the absence and presence of CT-DNA, respectively, K_{SV} is the Stern-Volmer fluorescence quenching constant and [Q] is the concentration of quencher. The value of K_{SV} was calculated 8.9×10^4 M^{-1} at 20°C (Fig. 5s).
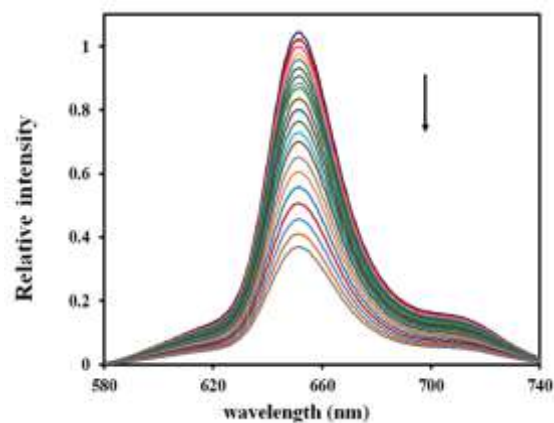
**Fig. 5.** Emission spectra of porphyrin **2**, upon increasing concentration of CT-DNA. [**2**]=7.81×10^{-6} M , [DNA] = $(0-2.52) \times 10^{-5}$ M, in Tris-HCl buffer, and $\lambda_{ex} = 426$ nm

RLS is an effective method for probing chromophore aggregation on nucleotide surfaces [45] and also for further accurate comprehension of binding mode [46]. The RLS spectra are depicted in Fig. 6. Upon CT-DNA addition, slight changes appeared in the RLS spectra. At low $\frac{[DNA]}{[porphyrin]}$ molar ratio, a little increase in the scattered light intensity (SLI) was observed in the region from 300 to 700 nm because of aggregations of desired porphyrins on the surface of DNA. Then with higher addition of CT-DNA, the SLI spectra was diminished because of binding monomers to CT-DNA instead of forming aggregates [47].
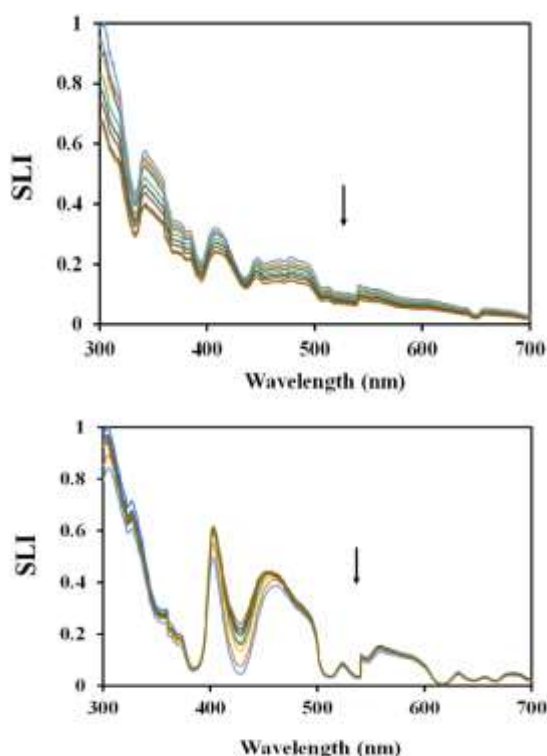
Fig. 6. RLS spectra of the solutions containing porphyrin (4.15 μM) in the presence of different concentrations of CT-DNA, **a)** [DNA] = $(0\text{-}1.71) \times 10^{-5}$ M, **b)** [DNA] = $(0\text{-}1.96) \times 10^{-5}$ M
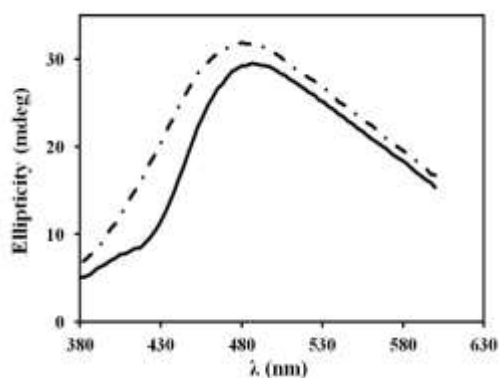
**Fig. 7.** Induced CD spectra of porphyrins **2** (**.-**) and **3** (**-**) in the presence of DNA at [porphyrin]/[DNA] ratios of 0.9 in the Soret region

Circular dichroism technique has been extensively used to understand the binding modes of a molecule to DNA [46]. Porphyrins **2** and **3** are an achiral molecule, so in the absence of DNA wasn't shown any ellipticity in the visible range. Upon interaction with CT-DNA and placing in a chiral environment, induced circular dichroism (ICD) peaks are appeared in Soret bands (Fig. 7). This occurrence can be explained that the origin of the induced CD arises from the coupling of the transition moments of achiral porphyrin, and chirally arranged nucleobases transition or along the

excitonic interaction of the DNA with porphyrin. The shape and magnitude of the induced CD give information about the binding mode [48]. The intercalative and outside binding mode are characterized by negative and the positive or zero ICD-spectra, respectively. Porphyrins **2** and **3** upon binding to CT-DNA indicated positive peaks at around 486 and 495 nm, respectively. The appearance of the positive ICD band suggested that these porphyrins bind to CT-DNA through outside binding mode, which is consistent with the above result.

The obtained spectroscopy results showed that these porphyrins bound to CT-DNA via groove binding mode with high affinity. [66]. The obtained results are in good accordance with previous studies. The last investigations exhibited that 5,10,15,20-tetrakis(4-methyl-pyridyl)porphyrin (TMPyP) and Cu(II) complex (CuTMPyP) were intercalated into CT-DNA base pairs with the binding constant 1.10×10^7 and 4.29×10^5 M^{-1}, respectively [49, 50]. In our previous study, we found that 5-(1-dodecyl pyridynium-4-yl)- 10, 15, 20- tris (1-methyl pyridynium-4-yl)- 21H, 23H- porphyrin tetra chloride (MDTMPyP) and its Cu (II) complex (CuMDTMPyP) were intercalated into CT-DNA through insertion of the planar aromatic ring into base pairs of DNA with the binding constant of 8.3×10^5 and 2.4×10^5 M^{-1} at 20°C, respectively [27]. But in the present work, MHxTB and CuMHxTB were bound to DNA by an outside binding mode and electrostatic interaction with the binding constant of 8.7×10^4 and 7.6×10^4 M^{-1}, respectively. These result showed that the DNA binding mechanism to porphyrin has been easily modified by changing the peripheral substituents. Actually, the planarity of the porphyrin ring was changed by increasing the length of the carbon chain in the porphyrin meso substituents and also the bulky group substitution was affected on the DNA binding with porphyrin.
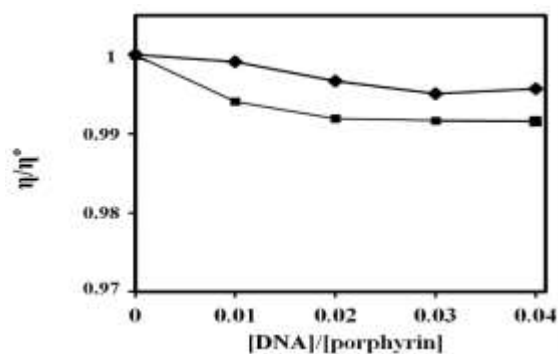
Fig. 8. Effect of increasing amounts of porphyrins **2** (■) and **3** (♦) on the relative viscosity of CT-DNA (100 µM) in Tris-HCl buffer solution. (r= [DNA]/[porphyrin], η^0 and η are the specific viscosity contributions of DNA in the absence and in the presence of the porphyrin, respectively

3.3. Measurements of viscosity

Measurements of viscosity DNA is an accurate method for determining the binding nature of porphyrins to DNA [51]. In the classical intercalation model, an increase in the relative viscosity of DNA is observed, which ascribed to lengthen the DNA duplex due to inserting small molecules between the base pairs of DNA [49]. In the outside binding model, a slight or no changes are observed in the effective length of DNA, which ascribed to bend or torsion in the DNA [52]. A plot of η/η^0 versus binding ratio are depicted in fig. 8. The obtained results show that the addition of porphyrins **2** and **3** had a little and insignificant effect on the relative viscosity of CT-DNA, and suggested that these porphyrins may bind to CT-DNA with an outside binding mode.

3.4. Molecular docking

Molecular docking is an extremely attractive technique that can be applied to predict the preferred orientation of porphyrins in interaction with DNA to form a stable complex [53]. Also, this method identified the binding energy and binding modes of porphyrin with DNA. In this process, the optimized geometry of porphyrins was docked into DNA fragments. The structure of porphyrins was kept flexible, and DNA structure was considered fix to achieve the most appropriate orientation and the best energy binding. The most stable conformation of the interaction of desired porphyrins with DNA was depicted in fig. 9 and docking analysis was listed in Table 1s. The binding energy of Porphyrins **2** and **3** were calculated -3.16 and -2.79 kcal/mol, respectively. However, electrostatics interaction is less than van der Waals in magnitude, but is the dominant force in defining the orientation of interaction. The obtained docking results confirmed our experimental findings that these porphyrins bound to DNA through groove binding mode.
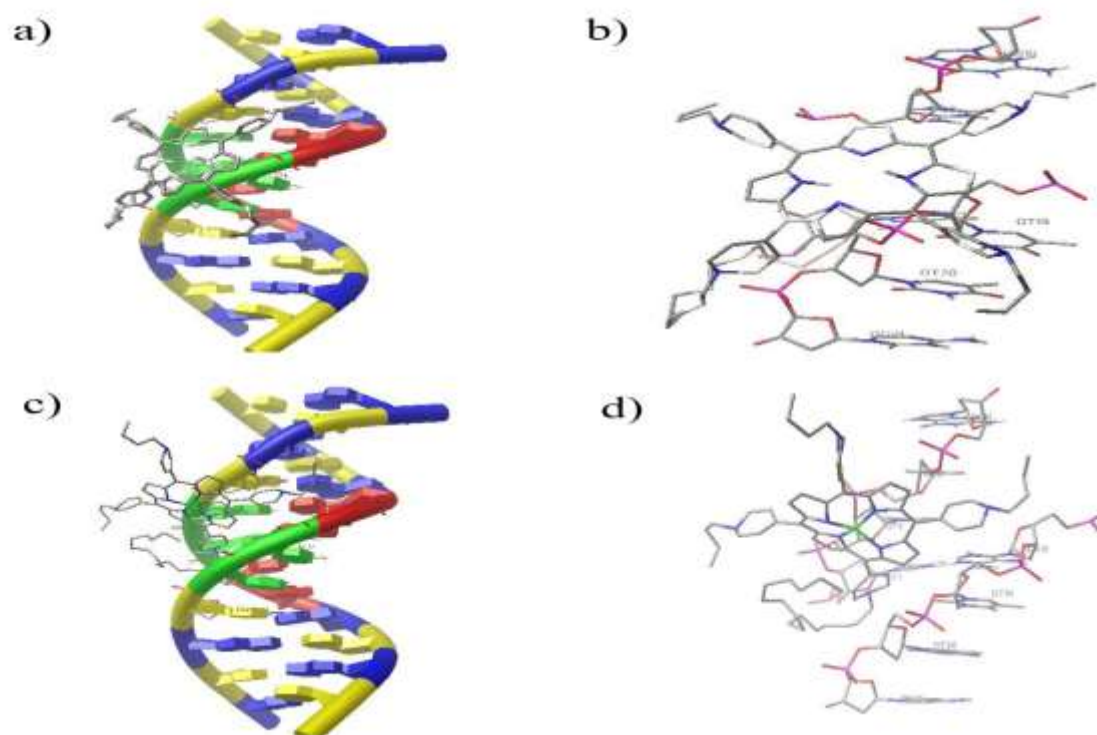
Fig. 9. Molecular docking results of porphyrin **2** (a) and porphyrin **3** (c) bound to DNA: deoxy adenine (DA) is red, deoxy cytosine (DC) is yellow, deoxy guanine (DG) is blue and deoxy thymine (DT) is green. Docking pose of porphyrin **2** (b), and porphyrin **3** (d)

4. conclusion

In this study, a water-soluble cationic asymmetric porphyrin, 5-(1-Hexadecyl pyridinium-4-yl)-10, 15, 20-tris (1-Butyl pyridinium-4-yl) Porphyrin Chloride (MHxTB), and its copper (II) derivative have been prepared and characterized spectroscopic methods. Then the interactions of these synthetic porphyrins with CT-DNA have been studied by various spectroscopic techniques, molecular docking, and viscosity measurements. The monitoring of the changes in visible absorbance spectra, showed that porphyrin **2** and **3** bound to CT-DNA with the binding constant (K_b) of 8.7×10^4 and $7.6 \times 10^4\,M^{-1}$ at 20°C, respectively. The obtained result confirm the high binding energy of these porphyrins with DNA, which is comparable to the other cationic porphyrins [54, 55]. Also, the binding constant was reduced to our earlier work due to the bulky group substitution [27]. Furthermore, molecular docking studies and spectroscopic investigations on the interaction of the mentioned porphyrins with CT-DNA suggested that these porphyrins bound to CT-DNA through outside binding mode.

References

[1] G.I. Cárdenas-Jirón, L. Cortez, *J. Mol. Model.* **19** (2013) 2913.

[2] C.W. Lee, H.P. Lu, C.M. Lan, Y.L. Huang, Y.R. Liang, W.N. Yen, Y.C. Liu, Y.S. Lin, E.W.G. Diau, C.Y. Yeh, *Chem.: A Eur. J.* **15** (2009) 1403.

[3] K. Alenezi, A. Tovmasyan, I. Batinic-Haberle, L.T. Benov, *Photodiagnosis Photodyn Ther.* **17** (2017) 154.

[4] W.-B. Huang, W. Gu, H.-X. Huang, J.-B. Wang, W.-X. Shen, Y.-Y. Lv, J. Shen, *Dyes Pigm.* **143** (2017) 427.

[5] X. Liang, X. Li, L. Jing, X. Yue, Z. Dai, *Biomaterials* **35** (2014) 6379.

[6] J.H. Zagal, S. Griveau, K.I. Ozoemena, T. Nyokong, F. Bedioui, *J. Nanosci. Nanotechnol.* **9** (2009) 2201.

[7] V. Jeyalakshmi, S. Tamilmani, R. Mahalakshmy, P. Bhyrappa, K.R. Krishnamurthy, B. Viswanathan, *J. Mol. Catal. A: Chem.* **420** (2016) 200.

[8] K. Garg, R. Shanmugam, P.C. Ramamurthy, *Carbon* **122** (2017) 307.

[9] L. Lvova, C. Di Natale, R. Paolesse, *Sens. Actuator B-Chem.* **179** (2013) 21.

[10] T. Higashino, S. Nimura, K. Sugiura, Y. Kurumisawa, Y. Tsuji, H. Imahori, *ACS Omega* **2** (2017) 6958.

[11] M. Hebenbrock, , D. González-Abradelo, C. A. Strassert, *J. Müller, Z. Anorg. Allg. Chem.* **644** (2018) 671.

[12] D.-F. Shi, R.T. Wheelhouse, D. Sun, L.H. Hurley, *J. Med. Chem.* **44** (2001) 4509.

[13] G. Mező, L. Herényi, J. Habdas, Z. Majer, B. Myśliwa-Kurdziel, K. Tóth, G. Csík, *Biophys. Chem.* **155** (2011) 36.

[14] M. Amiri1, M. Fazli, D. Ajloo, G. Grivani, *J. Appl. Chem.* **14** (2019) 75.

[15] R. Kuroda, H. Tanaka, *J. Chem. Soc., Chem. Commun.* **13** (1994) 1575.

[16] V.M. De Paoli, S.H. De Paoli, I.E. Borissevitch, A.C. Tedesco, *J. Alloys Compd.* **344** (2002) 27.

[17] V.G. Barkhudaryan, G.V. Ananyan, *J. Biomol. Struct. Dyn.* **33** (2015) 88.

[18] K. Bütje, J.H. Schneider, K. Nakamoto, J.-J.P. Kim, Y. Wang, S. Ikuta, *J. Inorg. Biochem.* **37** (1989) 119.

[19] L.A. Lipscomb, F.X. Zhou, S.R. Presnell, R.J. Woo, M.E. Peek, R.R. Plaskon, L.D. Williams, *Biochemistry* **35** (1996) 2818.

[20] M. Sari, J. Battioni, D. Dupre, D. Mansuy, J.B. Le Pecq, *Biochemistry* **29** (1990) 4205.

[21] M. Bennett, A. Krah, F. Wien, E. Garman, R. Mckenna, M. Sanderson, S. Neidle, *Proc. Natl. Acad. Sci.* **97** (2000) 9476.

[22] D.H. Tjahjono, S. Mima, T. Akutsu, N. Yoshioka, H. Inoue, *J. Inorg. Biochem.* **85** (2001) 219.

[23] N. Shahabadi, S. Kashanian, Z. Ahmadipour, DNA Cell Biol. 30 (2011) 187.

[24] Y. Ni, M. Wei, S. Kokot, *Int. J. Biol. Macromol.* **49** (2011) 622.

[25] W.H. Lawton, E.A. Sylvestre, *Technometrics* **13** (1971) 617.

[26] E. Reddi, M. Ceccon, G. Valduga, G. Jori, J.C. Bommer, F. Elisei, L. Latterini, U. Mazzucato, *Photochem. Photobiol.* **75** (2002) 462.

[27] R. Aleeshah, S.Zabihollahzadeh Samakoosh, A. Eslami, *J. Iran Chem. Soc.* **16** (2019) 1327.

[28] S. Zakavi, A.G. Mojarrad, T.M. Yazdely, *Macroheterocycles* **5** (2012) 67.

[29] M. Reichmann, S. Rice, C. Thomas, P. Doty, *J. Amer. Chem. Soc.* **76** (1954) 3047.

[30] M. Aminzadeh, A. Eslami, R. Kia, R. Aleeshah, *J. Mol. Struct.* **1165** (2018) 267.

[31] R. Tauler, Chemom. *Intell. Lab. Syst.* **30** (1995) 133.

[32] M. Maeder, *Anal. Chem.* **59** (1987) 527.

[33] A. de Juan, R. Tauler. Crit. Rev, *Anal. Chem.* **36** (2006) 163.

[34] J. Jaumot, R. Gargallo, A. de Juan, R. Tauler, Chemom. *Intell. Lab. Syst.* **76** (2005) 101.

[35] R. Tauler, A. Smilde, B. Kowalski, *J. Chemom.* **9** (1995) 31.

[36] R. Tauler, B. Kowalski, S. Fleming, *Anal. Chem.* **65** (1993) 2040.

[37] C.G. Ricci, P.A. Netz, *J. Chem. Inf. Model.* **49** (2009) 1925.

[38] W. J. Hehre, *Acc. Chem. Res.* **9** (1976) 399.

[39] G.M. Morris, D.S. Goodsell, R.S. Halliday, R. Huey, W.E. Hart, R.K. Belew, A.J. Olson. *J. Comput. Chem.* **19** (1998) 1639.

[40] C. Pérez-Arnaiz, N. Busto, J. Santolaya, J.M. Leal, G. Barone, B. García, *Biochim. Biophys. Acta* **1862** (2018) 522.

[41] S. Bhattacharya, G. Mandal, T. Ganguly, *J. Photochem. Photobiol., B* **101** (2010) 89.

[42] G. Pratviel, *Coord. Chem. Rev.* **308** (2016) 460.

[43] M.T. Carter, M. Rodriguez, A.J. Bard, *J. Amer. Chem. Soc.* **111** (1989) 8901.

[44] J.R. Lakowicz, G. Weber, *Biochemistry* **12** (1973) 4161.

[45] S. Gandini, I. Borissevitch, J. Perussi, H. Imasato, M. Tabak, *J. Lumin.* **78** (1998) 53.

[46] N.C. Sabharwal, O. Mendoza, J.M. Nicoludis, T. Ruan, J.-L. Mergny, L.A. Yatsunyk, *J. Biol. Inorg. Chem.* **21** (2016) 227.

[47] N. Rasouli, F. Fateminasab, *Phys. Chem. Res.* **3** (2015) 205.

[48] R.F. Pasternack, *Chirality* **15** (2003) 329.

[49] R. Fiel, J. Howard, E. Mark, N.D. Gupta, *Nucleic Acids Res.* **6** (1979) 3093.

[50] J. Li, Y. Wei, L. Guo, C. Zhang, Y. Jiao , S.Shuang, C. Dong, *Talanta*, **76** (2008), 34-39.

[51] A. Laesecke, J.L. Burger*, Biorheology* **51** (2014) 15.

[52] V.G. Barkhudaryan, G.V. Ananyan, Y.B. Dalyan, S.G. Haroutiunian, *J. Porphyr. Phthalocyanines* **18** (2014) 594.

[53] M. Arba, R.E. Kartasasmita, D.H. Tjahjono, *J. Biomol. Struct. Dyn.* **34** (2016) 427.

[54] M.I. Kwak, B.R. Jeon, S.K. Kim, Y.J. Jang, *ACS Omega* **3** (2018) 946.

[55] C. Romera, L. Sabater, A. Garofalo, I. M. Dixon, G. Pratviel, *Inorg. Chem.* **49** (2010) 8558.